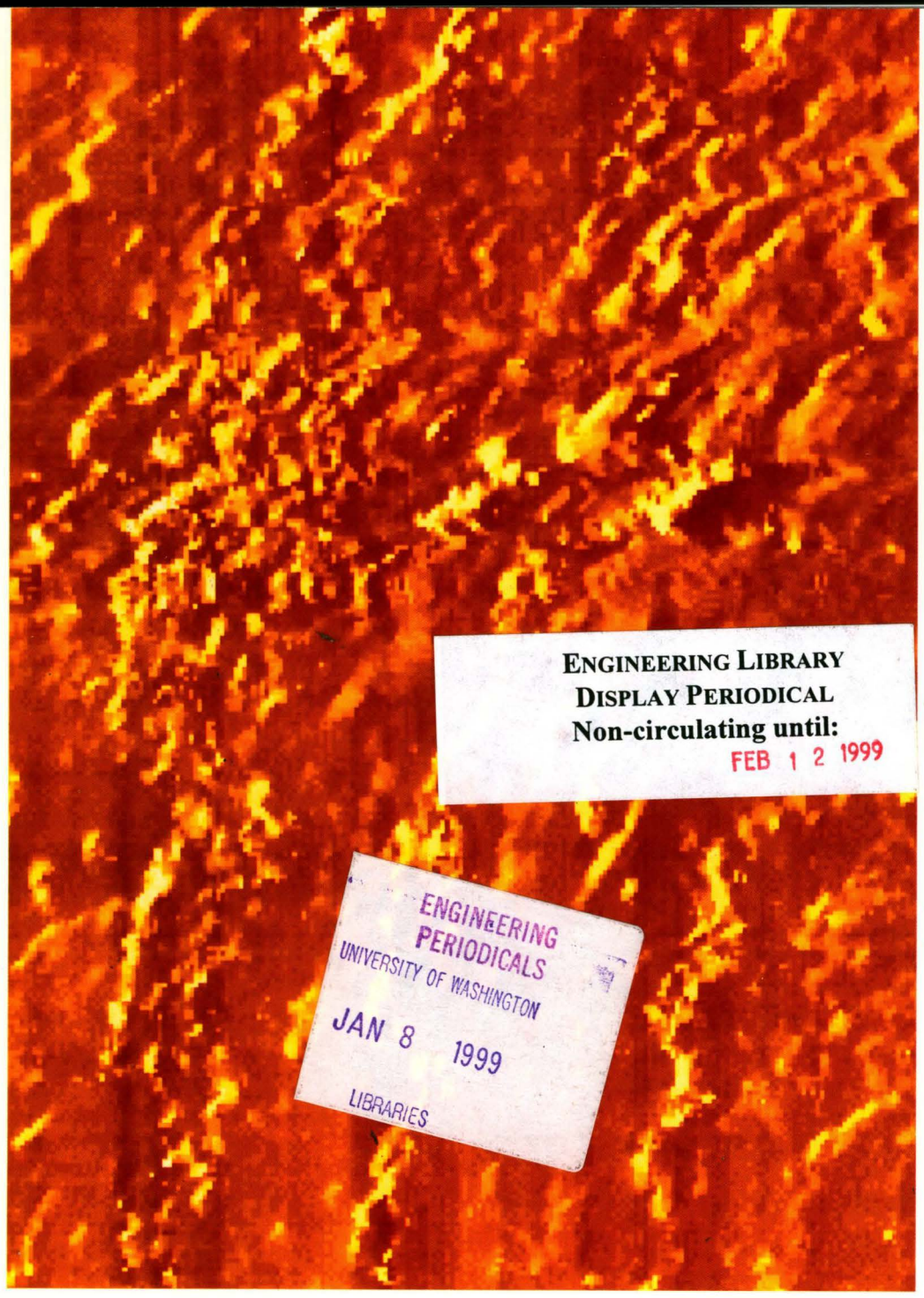

journal

of the American Ceramic Society

Incorporating Advanced Ceramic Materials and Communications

Volume 81 Number 12 December 1998

Journal
of the American Ceramic Society
Incorporating Advanced Ceramic Materials and Communications

ISSN 0002-7820
Volume 81
Number 12
December 1998

Instructions for preparation of papers are published in the December Issue of the *Journal*.

The *Journal of the American Ceramic Society* contains records of original research that provide or lead to fundamental principles of ceramics. Published papers explore mechanisms, structures, and behaviors as they relate to ceramic materials and principles of ceramics. Reports of discovery of new phases, phase relationships, and microstructures apply to a broad class of materials and processes, and reports of modeling are founded on basic mechanisms. Articles on the development, fabrication, and application of advanced ceramic and composite materials are of technical importance. The Communications section contains brief reports of a scientific or technical nature about new ideas and theories relevant to ceramic science; it also contains comments regarding previously published papers.

Editorial and Subscription Offices: P.O. Box 6136, Westerville, OH 43086-6136; Telephone (614) 794-5833; and Telefax (614) 794-5822. Annual North American subscription rates, including delivery, are: member, $92; list $425. Annual international subscription rates, including delivery, are: member, $172; list $505. Air mail is the standard delivery method to international customers. Libraries may call for package pricing. Single copies are $24 for members and $65 list plus postage and handling. Published monthly twelve times a year. Printed in the United States of America. POSTMASTER: Please send address changes to JOURNAL OF THE AMERICAN CERAMIC SOCIETY, P.O. Box 6136, Westerville, OH 43086-6136. Periodicals postage paid at Westerville, OH, and additional mailing offices. Allow six weeks for address changes.

The *Journal of the American Ceramic Society* is listed in Current Contents.

COVER PHOTOGRAPH: Magnetic force microscopy image of superconducting current flow (J = 100 A/cm^2) in a thick film at 60–65 K. See feature article by Dawn Bonnell, "Local Structure and Properties of Oxide Surfaces: Scanning Probe Analyses of Ceramics," this issue, pages 3049–70.

TABLE OF CONTENTS

VOLUME 81, 1998

February [2]

Centennial Feature

Articles

Communications

April [4]

Centennial Feature

Feature

Articles

May [5]

Centennial Feature

Articles

Communications

June [6]

Centennial Feature

Articles

Communications

August [8]

Centennial Feature

Feature

Articles

Communications

September [9]

Articles

Communications

October [10]

Articles

Communications

November [11]

Feature

Articles

December [12]

Feature

Articles

journal

J. Am. Ceram. Soc., 81 [12] 3141–49 (1998)

Improvement in Mechanical Properties of Powder-Processed $MoSi_2$ by the Addition of Sc_2O_3 and Y_2O_3

Yoshikazu Suzuki,† Peter E. D. Morgan,‡ and Koichi Niihara*,†

The Institute of Scientific and Industrial Research, Osaka University, Ibaraki, Osaka 567, Japan, and Rockwell Science Center, Thousand Oaks, California 91360

Additions of 1–20 mol% Sc_2O_3 or Y_2O_3 to $MoSi_2$ eliminate glassy SiO_2, which improves mechanical properties at both ambient and high temperatures. In particular, only 1 mol% ScO_3 additions dramatically enhance three-point bending strength from 521 to 1081 MPa. Vickers hardness, Young's modulus, fracture toughness, and high-temperature strength are also improved by this low level of additive. The improvement of mechanical properties is attributed to the formation of crystalline silicates: $Sc_2Si_2O_7$, $Y_2Si_2O_7$, Y_2SiO_5, and $Y_4Si_3O_{12}$, which are analyzed by XRD, SEM-EDS, and TEM-EDS methods.

I. Introduction

Molybdenum disilicide, $MoSi_2$, is an attractive candidate material for high-temperature structural applications because of its high melting point (2030°C), moderate density (6.27 g/cm^3), and excellent oxidation resistance.[1,2] Because of its intrinsically low ductility below the brittle-to-ductile transition temperature (BDTT: 900°–1400°C, depending on grain size and impurities),[1,3] powder processes are widely used for fabricating bulk $MoSi_2$ materials.[4] Because $MoSi_2$ powders that are prepared by fusing and crushing always contain a certain amount of oxygen, a monolithic $MoSi_2$ sintered body is actually composed of $MoSi_2$, Mo_5Si_3, and glassy SiO_2 phases. Mo_5Si_3, a low-silicide phase, is formed by a deviation from stoichiometry. With carbon impurity, the $Mo_{\leq 5}Si_3C_{\leq 1}$ Nowotny phase can also appear.[5–9] Inclusions, such as low silicides (here we include the $Mo_{\leq 5}Si_3C_{\leq 1}$ phase as a type of low silicide) and glassy SiO_2, affect various properties of $MoSi_2$. Low silicides have less oxidation resistance than $MoSi_2$,[10] but they can strengthen $MoSi_2$ as second-phase reinforcements.[11] While dispersion of low silicides in $MoSi_2$ compacts positively affects mechanical properties, glassy SiO_2 always affects them negatively.[11,12] The glassy SiO_2 phase forms discrete regions in $MoSi_2$ sintered bodies mainly at triple points,[8–9,11–13] as opposed to Si_3N_4, where glassy SiO_2 wets two-grain boundaries and triple points as layers. Nevertheless, glassy SiO_2 in $MoSi_2$ sintered bodies promotes creep by grain-boundary sliding, as in Si_3N_4, as it softens at high temperatures. Thus, glassy SiO_2 degrades mechanical properties, not only at room temperature, but also at high temperatures.[12]

The approaches to eliminate the siliceous grain-boundary phase can be classified into five categories: (1) reducing oxygen content in starting $MoSi_2$ powders, e.g., in-flight treatment in an argon–hydrogen plasma[4] and HF treatment;[14] (2) deoxidation during sintering by, e.g., carbothermal reduction[6–7,15] and hydrogen reduction;[16] (3) metathesis reaction during sintering, e.g., replacing SiO_2 by Al_2O_3 through aluminum metal addition;[17–19] (4) predominant oxidation of alloying element, e.g., aluminum, in starting powders;[9,20] and (5) double oxide formation during sintering.[8] For category (5), we have already reported that ZrO_2 (3Y) additions effectively decrease glassy SiO_2 in $MoSi_2$ sintered bodies by forming the more stable and crystalline double oxide $ZrSiO_4$.[8] Various mechanical properties are considerably improved by $ZrSiO_4$ formation and perhaps by the transformation toughening of unreacted ZrO_2.

In this study, we extended the *in situ* double oxide formation method to other oxide additives. C-rare-earth-structured oxides, Sc_2O_3 and Y_2O_3, were selected as additives because they have high reactivity with SiO_2 to form very refractory double oxides, i.e., $Sc_2Si_2O_7$ (mp, 1860°C), Sc_2SiO_5 (mp, 1950°C), $Y_2Si_2O_7$ (peritectic point, 1775°C), and Y_2SiO_5 (mp, 1980°C).[21,22] To clarify the effects of grain-boundary phases, we preferred to use a fine $MoSi_2$ powder (~1 μm) with rather high oxygen content (1.21 wt%). R_2O_3 (R = Sc and Y) powders (1–20 mol%) were added to the $MoSi_2$ powder so the effects of double oxide formation and second phase dispersion of excess, unreacted R_2O_3 in the $MoSi_2$ bodies could be examined.

Morgan *et al.*[23,24] previously studied the effects of Sc_2O_3 addition on Si_3N_4 and reported that oxidation resistance and creep resistance were significantly improved by the easy crystallization of the $Sc_2Si_2O_7$ phase (also known as the mineral thortveitite); these observations were confirmed in later works.[25,26] We conjectured similar positive effects for the Mo–Si–Sc–O system because both Si_3N_4 and $MoSi_2$ have siliceous grain-boundary phases that greatly affected various mechanical properties. For Y_2O_3, Kulenko *et al.*[27] reported on the $MoSi_2$–Y_2O_3 system prepared by pressureless sintering. The main purpose of their study was to increase the electrical resistivity of $MoSi_2$ bodies without necessarily affecting the mechanical properties. They examined relatively high amounts of Y_2O_3 (10%–50%, presumably weight fraction, as the authors did not clearly state), and mechanical properties were scarcely mentioned. Research on $MoSi_2$–Y_2O_3 composites was also conducted by Zalkind *et al.*,[28] who demonstrated that the $MoSi_2$–Y_2O_3 composites showed good corrosion resistance to melts of fuel slag, indicating the potential benefits of the $MoSi_2$–Y_2O_3 system.

This initial investigation shows that even minor amounts of Sc_2O_3 and Y_2O_3 additions (1 mol%) are effective in greatly improving mechanical properties of $MoSi_2$-based materials.

II. Experimental Procedure

(1) Sample Preparation

Starting materials were $MoSi_2$ (1.01 μm, Japan New Metals Co., Ltd.), Sc_2O_3 and Y_2O_3 (~2 μm, Kojundo Chemical Laboratory Co., Ltd.). The R_2O_3 additions in this investigation were restricted to 1–20 mol% because a larger amount of oxides

J. J. Petrovic—contributing editor

Manuscript No. 190747. Received August 28, 1997; approved February 23, 1998.
Supported by the Japan Ministry of Education, Science, Sports, and Culture under Grant-in-Aid for Science Research No. 08044150 and 09450262, and for JSPS Research Fellowships.

*Member, American Ceramic Society.
†Osaka University.
‡Rockwell Science Center.

might degrade the high-temperature mechanical properties. The chemical analysis of the starting $MoSi_2$ powder is shown in Table I. Spectrochemical analysis revealed that the major impurities were 1.21 wt% oxygen, 0.20 wt% carbon, and 0.21 wt% iron. The high oxygen level was associated with the fine particle size (1.01 μm) of the $MoSi_2$ powder. Table II shows the composition of the $MoSi_2$ starting powder calculated from Table I, assuming that the phases in the powder were $MoSi_2$, Mo_5Si_3, glassy SiO_2, free carbon, and Fe_2O_3. This result assumed that 1.21 wt% oxygen in the $MoSi_2$ powder was equivalent to ~6 vol% of glassy SiO_2. $MoSi_2$ and additive oxide powders were wet ball-milled with ZrO_2 balls for 24 h in *n*-hexane, which was used to avoid the mechanochemical oxidation by usual alcohol solvents, as reported for Si_3N_4.[29] Nominal compositions of the powder mixture are summarized in Table III. The mixture was packed into carbon dies, coated with BN, and hot-pressed at 1600°C under an applied pressure of 30 MPa for 1 h under vacuum. The sintered disks, 44 mm in diameter and 5.0 mm thick, were cut, ground, and polished into rectangular bars 4 mm × 3 mm × 36 mm in size for three-point bending test.

(2) Evaluation Methods

Phase identification was conducted by X-ray diffraction (XRD) analysis. To minimize the anisotropic orientation effect, liquid paraffin was mixed with the pulverized specimen. The microstructure was characterized by scanning electron microscopy (SEM, Model S-5000, Hitachi, Tokyo, Japan) with energy dispersive X-ray spectrometry (EDS, Model EMAX-5770, Horiba, Tokyo, Japan) with the samples precoated with carbon. Transmission electron microscopy (TEM, Model H-8100, Hitachi) with EDS (Model PV9900, Phillips, Eindhoven, The Netherlands) was also used for the microstructural characterization. The bulk density was measured by the Archimedes method in toluene at room temperature; temperature corrections were always conducted for the density measurements. Young's modulus was determined by the resonance vibration method with the thickness correction. Five or six specimens in each case were subjected to three-point bending test (span: 30 mm, in air) to determine fracture strength up to 1300°C. The bending load was applied parallel to the hot-pressing axis with a crosshead speed of 0.5 mm/min. Hardness (H_V) was evaluated by Vickers indentation under conditions of 98 N load with loading duration of 15 s in air. Fracture toughness (K_{IC}) at room temperature was determined simultaneously by the indentation fracture (IF) method.[30] K_{IC} values were calculated using the following empirical equation for a median crack:

$$K_{IC} = 0.203(c/a)^{-3/2}H_V a^{1/2} \quad (1)$$

where c and a are the lengths of a median crack and half of a diagonal of an indentation, respectively.

III. Results

(1) Phase Analysis of Sc_2O_3-Containing Materials

Figure 1 shows the XRD patterns for (a) $MoSi_2$ with added Sc_2O_3 and (b) $MoSi_2$ with added Y_2O_3 hot-pressed bodies with increasing additive amounts. Because the XRD intensities of $MoSi_2$ are quite strong in comparison with those of other phases, the peak tops are truncated. XRD analysis of the phases in the sintered bodies is summarized in Table IV. XRD analysis indicates that the monolithic $MoSi_2$ body is composed of $MoSi_2$ (tetragonal, $C11_b$), a small amount of $Mo_{\leq 5}Si_3C_{\leq 1}$ (hexagonal, $D8_8$), and a trace of SiO_2 (cristobalite). The $Mo_{\leq 5}Si_3C_{\leq 5}$, Nowotny phase,[31] is the only stable Mo-Si-C ternary phase. TEM selected area diffraction analysis reveals that most of the SiO_2 exists as glassy phase; however, the cristobalite observed by XRD must be attributed to partial crystallization of glassy SiO_2. In the 1–2-mol%-Sc_2O_3–$MoSi_2$ sintered bodies, $Sc_2Si_2O_7$, thortveitite, (Sc_2O_3:SiO_2 = 1:2) is identified. $Sc_2Si_2O_7$ is a stable refractory compound (mp, 1860°C)[21] in the Sc_2O_3–SiO_2 binary system. $Sc_2Si_2O_7$ is reported to form readily in the hot-pressed Si_3N_4–SiO_2–Sc_2O_3 system also.[23–26] The cristobalite peak around $2\theta = 22°$ decreases (as expected) with increasing Sc_2O_3 content (0–5 mol%) as $Sc_2Si_2O_7$ forms with the inevitable reaction with glassy SiO_2. For the $MoSi_2$ with 5 mol% Sc_2O_3, most of the SiO_2 in the sintered body is converted to the silicate, because the cristobalite peak disappears and small peaks from unreacted Sc_2O_3 are observed. With higher Sc_2O_3 additions (10–20 mol%), the constituent phases are the same as in the 5-mol%-Sc_2O_3–$MoSi_2$ case; the amount of unreacted Sc_2O_3 simply increases. In the Sc_2O_3–SiO_2 binary system,[21] there should be another silicate, Sc_2SiO_5 (Sc_2O_3:SiO_2 = 1:1), when Sc_2O_3 content increases. However, the Sc_2SiO_5 phase is never observed in this experiment, as discussed later.

(2) Phase Analysis of Y_2O_3-Containing Materials

For $MoSi_2$ with 1–2 mol% Y_2O_3, the formation of the 1:2 silicate, i.e., $Y_2Si_2O_7$, is confirmed, similar to $Sc_2Si_2O_7$ formation in the $MoSi_2$–SiO_2–Sc_2O_3 system. Three polymorphs of $Y_2Si_2O_7$ phase are identified: β-phase (keiviite-(Y)), *y*-phase, and δ-phase. β-$Y_2Si_2O_7$ has the thortveitite-type crystal structure and is stable at high temperatures around the hot-pressing temperature (1600°C).[22,32] Dinger *et al.*[33] studied the crystallization behavior of the glasses in the Y_2O_3–SiO_2–AlN system and reported that *y*-$Y_2Si_2O_7$, δ-$Y_2Si_2O_7$, and β-$Y_2Si_2O_7$ phases were observed, with *y*-$Y_2Si_2O_7$ and δ-$Y_2Si_2O_7$ crystallizing at ~1000° and 1200°C, respectively, and β-$Y_2Si_2O_7$ crystallizing at higher temperatures. Because the hot-pressing time in this study is not long, it is perhaps not surprising that metastable polymorphs of $Y_2Si_2O_7$ remain in the sintered bodies. The intensity of the cristobalite peak at $2\theta = 22°$ also decreases with increasing Y_2O_3 content (0–5 mol%), similar to the Sc_2O_3 case. A trace of Y_2O_3 is also identified in the 1–2-mol%-Y_2O_3–$MoSi_2$, despite the presence of free SiO_2 presumably because of diffusion limitation and separation by the majority $MoSi_2$ matrix.

For $MoSi_2$ with 5 mol% Y_2O_3, $Y_2Si_2O_7$, unreacted SiO_2 and Y_2O_3 are observed in addition to $MoSi_2$ and $Mo_{\leq 5}Si_3C_{\leq 1}$. Furthermore, a notable peak at $2\theta = 32°$ is observed, which was never seen in the other specimens, and is identified as the 2:3 silicate $Y_4Si_3O_{12}$. According to the published phase diagram,[22] this phase is not stable below 1650°C; nevertheless, it appears here. Although it may cast some doubt on the veracity of this early diagram, it is not surprising that the formation of $Y_4Si_3O_{12}$ takes place, because the eutectoid temperature is only 50°C higher than the hot-pressing temperature (1600°C); thus, some impurity, pressure, and local temperature gradient (e.g., by a reaction heat) presumably affects the reactivity. For compacts with higher Y_2O_3 additions (10–20 mol%), SiO_2 and $Y_4Si_3O_{12}$ disappear, and Y_2SiO_5 (Y_2O_3:SiO_2 = 1:1) forms. The equivalent 1:1 silicate is not observed in the $MoSi_2$–SiO_2–Sc_2O_3 system.

Table I. Chemical Analysis of the $MoSi_2$ Starting Powder

	Mo†	Si	O	C	Fe
Content (wt%)	62.18	36.20	1.21	0.20	0.21

†Molybdenum content was calculated so that total content was 100%.

Table II. Calculated Composition of the $MoSi_2$ Starting Powder

	$MoSi_2$	Mo_5Si_3†	Glassy SiO_2	Free carbon‡	Fe_2O_3
Content (mol%)	91.20	0.90	5.10	2.50	0.30
Content (wt%)	94.00	3.40	2.10	0.20	0.30
Content (vol%)	90.90	2.50	5.70	0.50	0.40
Density (g/cm^3)	6.27	8.19	2.22	2.25	5.24

†Mo_5Si_3 increases with oxidation and reacts with carbon to form $Mo_{\leq 5}Si_3C_{\leq 1}$.
‡Some carbon can dissolve in SiO_2 glass.

Table III. Nominal Compositions of the Powder Mixture[†]

Sample No.	Composition (mol%)			Composition (wt%)[‡]			Composition (vol%)[§]		
	$MoSi_2$	Sc_2O_3	Y_2O_3	$MoSi_2$	Sc_2O_3	Y_2O_3	$MoSi_2$	Sc_2O_3	Y_2O_3
1	100			100.0			100.0		
2	99	1		99.1	0.9		98.5	1.5	
3	98	2		98.2	1.8		97.1	2.9	
4	95	5		95.4	4.6		92.8	7.2	
5	90	10		90.8	9.2		85.9	14.1	
6	85	15		86.2	13.8		79.3	20.7	
7	80	20		81.5	18.5		73.0	27.0	
8	99		1	98.5		1.5	98.2		1.8
9	98		2	97.1		2.9	96.4		3.6
10	95		5	92.8		7.2	91.1		8.9
11	90		10	85.8		14.2	83.0		17.0
12	85		15	79.2		20.8	75.4		24.6
13	80		20	72.9		27.1	68.4		31.6

[†]Assuming that the starting powders are pure $MoSi_2$, Sc_2O_3, and Y_2O_3. [‡]Formula weight: $MoSi_2$ = 152.111, Sc_2O_3 = 137.91, and Y_2O_3 = 225.81. [§]X-ray density: D_{MoSi_2} = 6.27 g/cm^3, $D_{Sc_2O_3}$ = 3.840 g/cm^3, and $D_{Y_2O_3}$ = 5.032 g/cm^3.

(3) Microstructure

Figure 2 shows typical SEM photographs on the polished surfaces of monolithic $MoSi_2$ and $MoSi_2$ with R_2O_3 additives: (a) monolithic $MoSi_2$; (b) 1, (c) 5, (d) 10, and (e) 20 mol% Sc_2O_3; (f) 1, (g) 5, (h) 10, and (i) 20 mol% Y_2O_3. In these figures, the dark regions are composed of the mixed oxides detailed in the phase analysis (not pores). The regions with light-gray contrast are the $Mo_{\leq 5}Si_3C_{\leq 1}$ phase. In the monolithic $MoSi_2$ sintered body, glassy SiO_2 particles with spherical or irregular shape are isolated, unlike in Si_3N_4 sintered bodies, where glassy SiO_2 is distributed as a grain-boundary film. The $Mo_{\leq 5}Si_3C_{\leq 1}$ phase is usually found next to glassy SiO_2 regions. This microstructure may be explained as follows: The starting $MoSi_2$ powder has oxidized glassy SiO_2 on the surfaces and a thin Mo_5Si_3 region below the SiO_2 layer.[34] During hot-pressing, the glassy SiO_2 becomes concentrated mainly at triple points, and the $Mo_{\leq 5}Si_3C_{\leq 1}$ is formed by reactions between Mo_5Si_3 and impurity carbon.[6,7] The carbon impurity arises from the powder used, the ball-milling solvent, and the CO gas from a die and a furnace element. SEM–EDS study reveals that scandium and yttrium elements appear predominantly in the SiO_2 pockets. Thus, it is inferred that the additives and SiO_2 react together at grain-boundary pockets. With higher additive content, the oxide phases become continuous, as seen in Figs. 2(d), (e), (h), and (i).

(4) Density

Figure 3 shows the variation of density of hot-pressed bodies with Sc_2O_3 and Y_2O_3 addition. The density of the monolithic $MoSi_2$ compact is 5.92 g/cm^3. This value is smaller than the theoretical density of the $MoSi_2$ phase determined by XRD (6.27 g/cm^3). Because almost no pores are observed by SEM for the $MoSi_2$ sintered body, the lower density is attributed to the formation of glassy SiO_2 with its rather low density (2.20 g/cm^3). For the Y_2O_3-added system, density increases then decreases with Y_2O_3 content. This suggests the formation of a higher-density phase compared to glassy SiO_2. With Sc_2O_3 addition, the density curve has a maximum at 5 mol% Sc_2O_3, also suggesting the formation of a higher-density phase. The density dependence is discussed later in detail.

(5) Mechanical Properties

Young's modulus dependence on Sc_2O_3 and Y_2O_3 content is shown in Fig. 4. The Young's modulus of the monolithic $MoSi_2$ compact is 372 GPa. This value is smaller than the theoretical Young's modulus of polycrystalline $MoSi_2$ calculated from the single crystal (440 GPa).[35] In general, Young's modulus is strongly affected by the presence of porosity.[36] However, because almost no pores are observed in the sintered body as mentioned above, the decrease in Young's modulus is explained by the formation of glassy SiO_2 phase. For both Sc_2O_3 and Y_2O_3 additions, Young's modulus indicates the maximum values at 5 mol% addition, the minimum additive composition to remove glassy SiO_2 in the sintered bodies. Because Young's moduli of Sc_2O_3 and Y_2O_3 are smaller than that of $MoSi_2$, 5 mol% addition results in the maximum values. The Young's modulus dependence is discussed further in the next section.

Figure 5 shows the variation of fracture strength with additive content. The strength value of monolithic $MoSi_2$ is 521 MPa. Fracture strength increases then decreases with increasing additive content. For both Sc_2O_3 and Y_2O_3 addition, maximum fracture strength is obtained for only 1 mol% addition. The strength values of $MoSi_2$ with 1 mol% Sc_2O_3 and Y_2O_3 are 1081 and 1028 MPa, respectively. These values are extremely high for $MoSi_2$-based materials.[2] At higher oxide phase contents, fracture strength decreases, perhaps because the oxides become connected in a larger potential flaw fracture origin. For 1 mol% addition, the total amount of oxide phase is still small, and oxide regions are discrete; the glassy SiO_2 has sufficiently reacted with the additive to form 1:2 silicate, apparently causing strengthening. Because only 1 mol% R_2O_3 additive is sufficient to greatly improve fracture strength, the use of expensive Sc_2O_3 may become more viable from a cost standpoint.

Figure 6 shows the variation of Vickers hardness with additive content. The change of Vickers hardness with additive content resembles that of Young's modulus. Hardness shows its maximum value at 5 mol% for both Sc_2O_3 and Y_2O_3 addition. This is attributed to the approach to total crystallization of the glassy phase. The decrease in hardness with higher additive content is due to the softness of unreacted Y_2O_3 or Sc_2O_3 additive.

Fracture toughness dependence on additive content is shown in Fig. 7. The variation of fracture toughness with additive content is similar to that of Young's modulus and Vickers hardness for the same reasons. Too much additive also decreases fracture toughness, also for the same reasons.

Figure 8 shows high-temperature strength of $MoSi_2$ with 1 mol% Sc_2O_3 and Y_2O_3. At >1100°C, both materials display plastic deformation without fracture. The values of two different monolithic $MoSi_2$ samples are also shown in the figure for reference: fine $MoSi_2$ is fabricated by hot-pressing a fine $MoSi_2$ powder (1.0 μm, almost identical to this experiment) at 1500°C, whose grain size is ~5 μm,[37] and coarse $MoSi_2$ is made by hot-pressing a coarse powder (several tens of micrometers, typical values for conventional $MoSi_2$) at 1700°C.[38] Because coarse-grained $MoSi_2$ contains less glassy phase, it maintains almost the same, albeit low, strength (~150 MPa) up to 1200°C. On the other hand, fine-grained $MoSi_2$ shows improved strength for the entire temperature range compared to coarse-grained $MoSi_2$, although strength degradation is observed above 800°C. The improvement of strength up to 800°C

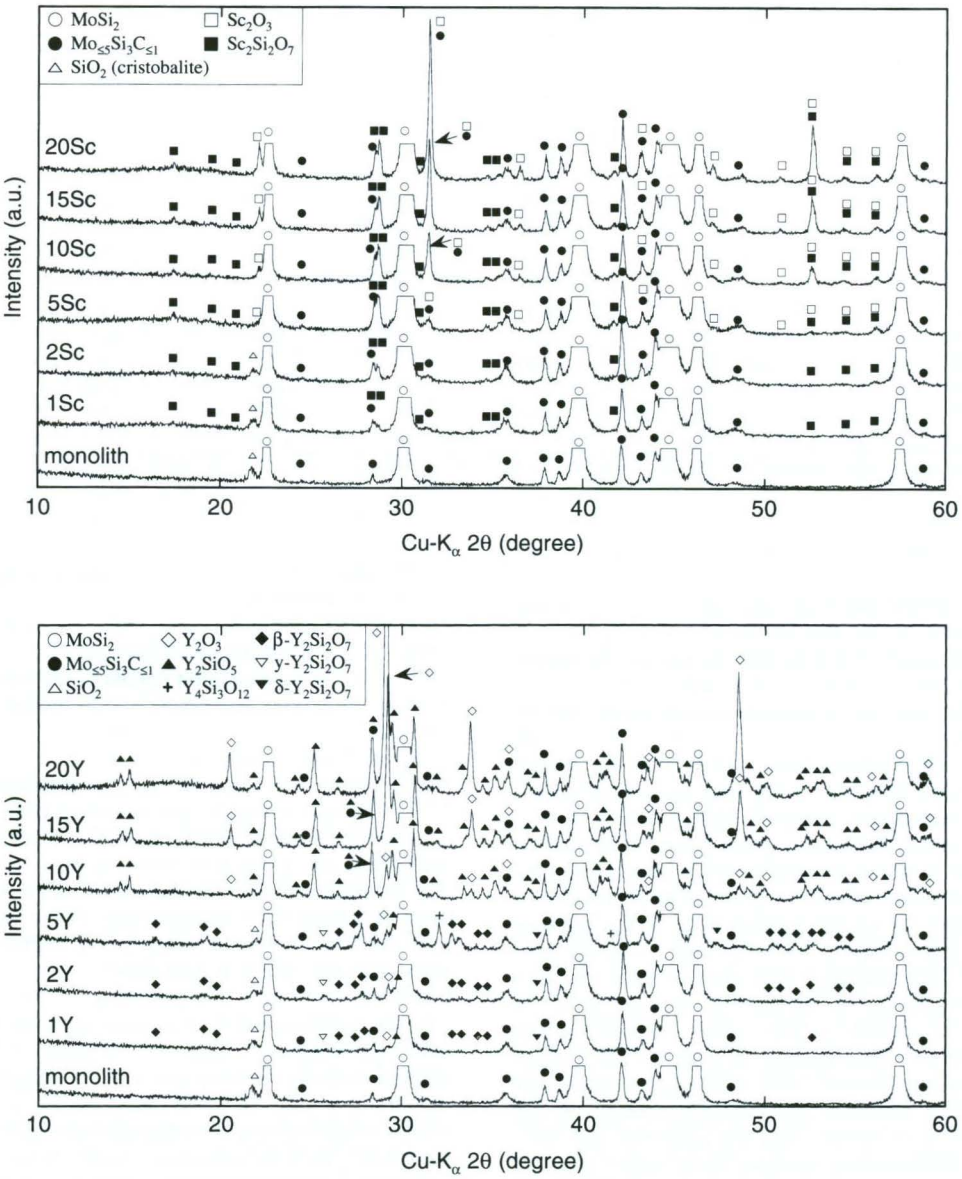

Fig. 1. XRD patterns for (a) $MoSi_2$–SiO_2–Sc_2O_3 and (b) $MoSi_2$–SiO_2–Y_2O_3 systems.

Table IV. Phase Contents of the Hot-Pressed Products in the $MoSi_2$–R_2O_3 (R = Sc and Y) Systems

Sample No.	Nominal starting composition (mol%)	Phases in product (identified by XRD)
1	$MoSi_2$	$MoSi_2$, $Mo_{\leq 5}Si_3C_{\leq 1}$, SiO_2[†]
2, 3	$MoSi_2$ + 1.2% Sc_2O_3	$MoSi_2$, $Mo_{\leq 5}Si_3C_{\leq 1}$, SiO_2,[†], $Sc_2Si_2O_7$
4	$MoSi_2$ + 5% Sc_2O_3	$MoSi_2$, $Mo_{\leq 5}Si_3C_{\leq 1}$, $Sc_2Si_2O_7$, (trace Sc_2O_3)
5, 6, 7	$MoSi_2$ + 10, 15, 20% Sc_2O_3	$MoSi_2$, $Mo_{\leq 5}Si_3C_{\leq 1}$, $Sc_2Si_2O_7$, Sc_2O_3
8, 9	$MoSi_2$ + 1.2% Y_2O_3	$MoSi_2$, $Mo_{\leq 5}Si_3C_{\leq 1}$,[†] SiO_2,[†] $Y_2Si_2O_7$, (trace Y_2O_3)
10	$MoSi_2$ + 5% Y_2O_3	$MoSi_2$, $Mo_{\leq 5}Si_3C_{\leq 1}$, SiO_2,[†] $Y_2Si_2O_7$, $Y_4Si_2O_7$, (trace Y_2O_3)
11, 12, 13	$MoSi_2$ + 10, 15, 20% Y_2O_3	$MoSi_2$, $Mo_{\leq 5}Si_3C_{\leq 1}$, Y_2SiO_5, Y_2O_3

[†]Cristobalite, partially crystallized from glassy SiO_2.

is due to the healing effect of the glassy phase (i.e., recovering of surface flaws), while the drop in strength near 1000°C is mainly due to the glassy phase allowing grain-boundary sliding. $MoSi_2$ with 1 mol% oxide additives shows much higher strength values (>750 MPa) up to 1100°C than conventional $MoSi_2$-based materials. However, because these materials still contain some unreacted glassy SiO_2, their strength declines around 1100°C, similar to the fine-grained $MoSi_2$. Further crystallization of glassy SiO_2 may somewhat improve strength above 1200°C.

IV. Discussion

(1) Difference of Phases Appearing between Two Systems

Interesting differences between the formed silicates with Sc_2O_3 and Y_2O_3 additions were mentioned in Section III (Fig. 1 and Table IV). Because there are limited thermodynamic data in the Sc_2O_3–SiO_2 and Y_2O_3–SiO_2 binary systems, we are basically limited to phase diagrams. Figures 9(a) and (b) show these for Sc_2O_3–SiO_2[21] and Y_2O_3–SiO_2 systems.[22]

For 1–5 mol% Y_2O_3 addition, some SiO_2 remains in the

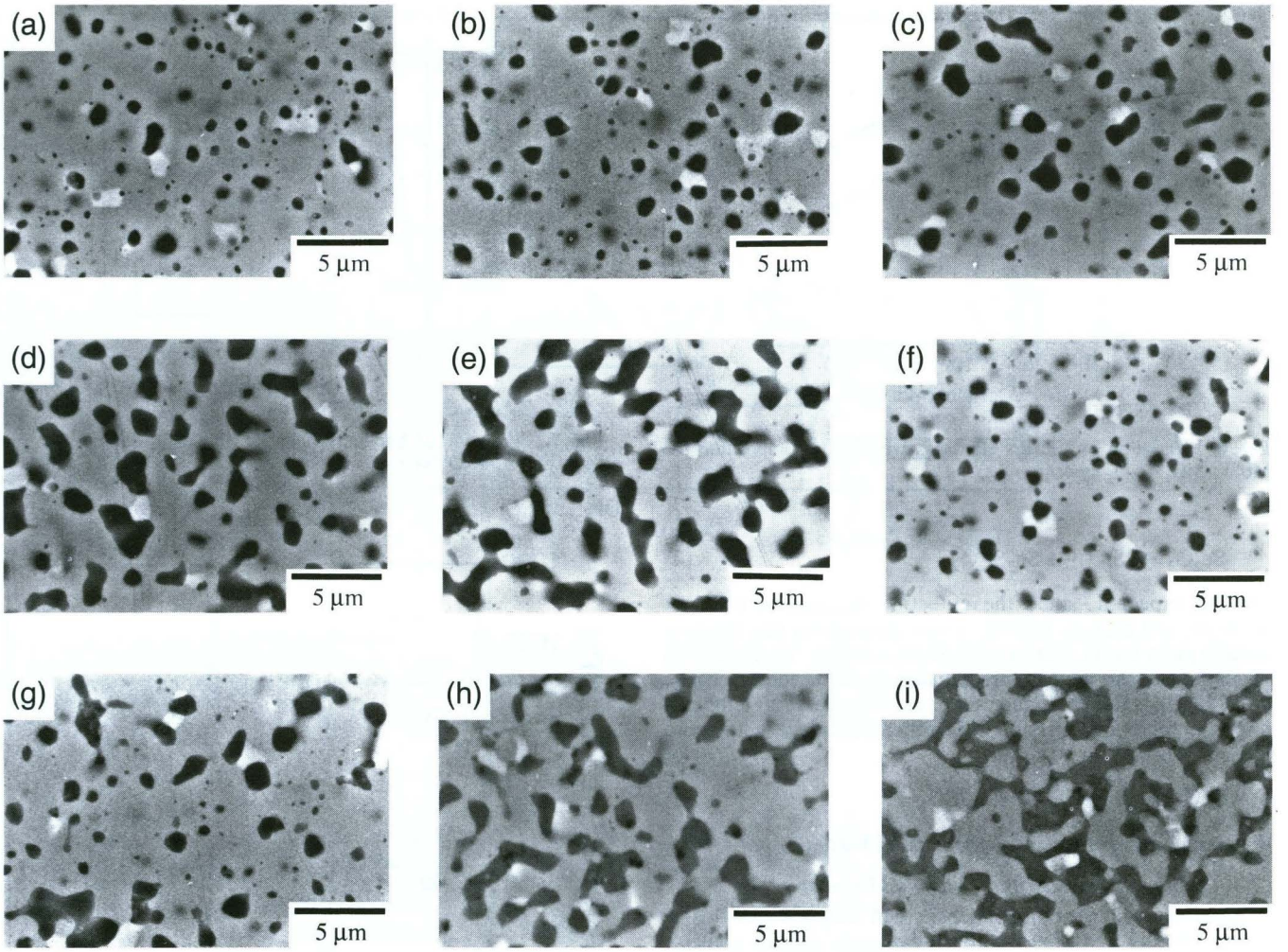

Fig. 2. SEM photographs of polished surfaces: (a) monolithic $MoSi_2$; (b) 1, (c) 5, (d) 10, and (e) 20 mol% Sc_2O_3; (f) 1, (g) 5, (h) 10, and (i) 20 mol% Y_2O_3.

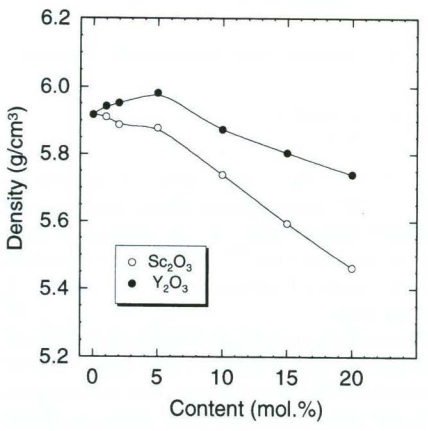

Fig. 3. Variation of density with R_2O_3 (R = Sc and Y) composition for $MoSi_2$–SiO_2–R_2O_3 system.

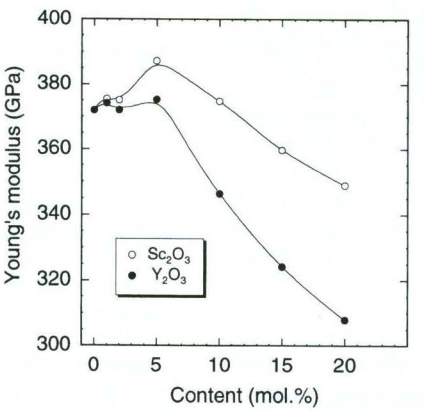

Fig. 4. Variation of Young's modulus with R_2O_3 composition for $MoSi_2$–SiO_2–R_2O_3 system.

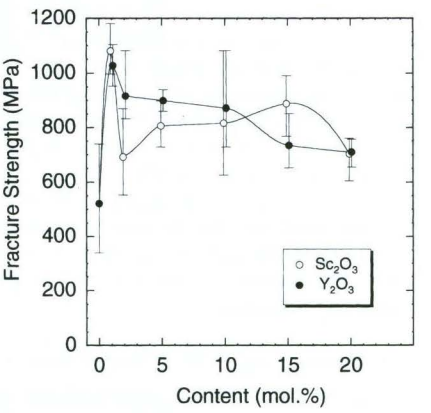

Fig. 5. Variation of fracture strength with R_2O_3 composition for $MoSi_2$–SiO_2–R_2O_3 system.

sintered bodies and $Y_2Si_2O_7$ appears as a crystalline phase. With greater Y_2O_3 addition (10–20 mol%), SiO_2 disappears and Y_2SiO_5 phase is formed, replacing $Y_2Si_2O_7$ phase, as anticipated from Fig. 9(b), with some excess Y_2O_3 remaining.

For Sc_2O_3 addition, the lower additive content (1–5 mol%) has almost the same results as Y_2O_3 addition (i.e., formation of 1:2 silicate, $Sc_2Si_2O_7$), but, on the other hand, higher additive content (10–20 mol%) does not produce 1:1 silicate, Sc_2SiO_5. The hot-pressing temperature used in this study is 1600°C, and this temperature is evidently high enough for the following reaction to occur:

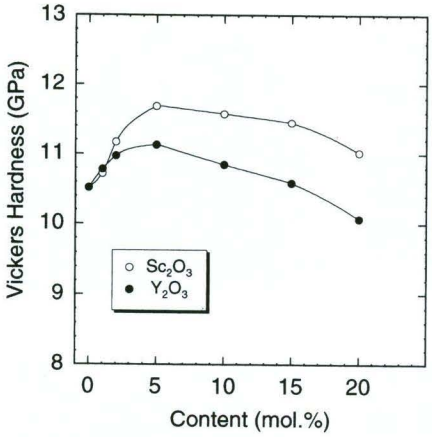

Fig. 6. Variation of Vickers Hardness with R_2O_3 composition for $MoSi_2$–SiO_2–R_2O_3 system.

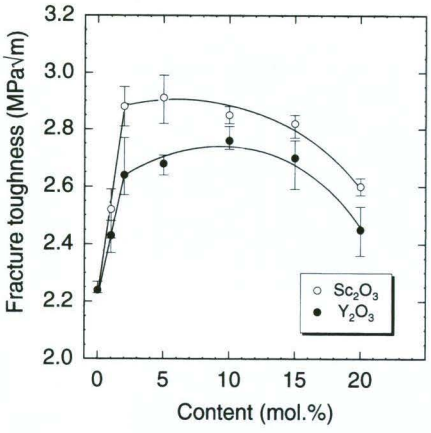

Fig. 7. Variation of fracture toughness with R_2O_3 composition for $MoSi_2$–SiO_2–R_2O_3 system.

$$Sc_2O_3 + 2SiO_2 \rightarrow Sc_2Si_2O_7 \quad (2)$$

This is expected, since the eutectic temperature between $Sc_2Si_2O_7$ and SiO_2 at 1660°C is near enough for this reaction to take place easily. For greater Sc_2O_3 content (10–20 mol%) when the eutectic temperature between Sc_2SiO_5 and $Sc_2Si_2O_7$, at 1770°C, is much higher than the hot-pressing temperature, the following reaction evidently takes place with more difficulty:

$$Sc_2O_3 + Sc_2Si_2O_7 \rightarrow 2Sc_2SiO_5 \quad (3)$$

suggesting a larger kinetic or nucleation barrier.

(2) Change of Density and Young's Modulus

As is shown in Section III, density and Young's modulus of sintered bodies increases then decreases with additive content. To discuss such changes, densities and Young's moduli of constituent phases are listed in Table V.[35,39–49] The density of monolithic $MoSi_2$ sintered body in this study is 5.92 g/cm^3, which is lower than the theoretical density of 6.27 g/cm^3 calculated from XRD;[39] thus, the decrement of density must be attributed to the formation of low density (2.20 g/cm^3) glassy SiO_2. As discussed in the phase analysis part, some cristobalite exists that spontaneously crystallizes from glassy SiO_2. The density of cristobalite is 2.33 g/cm^3;[41] therefore, the difference in density between glassy SiO_2 and cristobalite is small. Although the density of $Mo_{\leq 5}Si_3C_{\leq 1}$ phase depends on its chemical composition, a typical value for $Mo_{4.8}Si_3C_{0.6}$ is reported as 7.891 g/cm^3,[40] which is slightly higher than that of $MoSi_2$. Because the content of $Mo_{\leq 5}Si_3C_{\leq 1}$ phase is small (~3 vol% detected through image analysis of SEM photographs), it can be neglected for the density calculation. Supposing that the $MoSi_2$ sintered body is composed of only $MoSi_2$ and glassy SiO_2, the density of the sintered body is calculated by the following equation:

$$D_{\text{sintered body}} = (1 - V_{SiO_2})D_{MoSi_2} + V_{SiO_2}D_{SiO_2} \quad (4)$$

where V and D represent volume fraction and density. $D_{\text{sintered body}}$, D_{MoSi_2}, and D_{SiO_2} are 5.92, 6.27, and 2.22 g/cm^3, respectively. V_{SiO_2} is calculated as 8.6% by Eq. (4), in good agreement with the volume fraction from image analysis (~8.5%). This value is somewhat larger than the total oxide content in the starting $MoSi_2$ powder (~6 vol%) as listed in Table II. It may be attributed to more oxidation of fresh surface by ball milling.

The volume changes (ΔV) associated with the reactions

$$Sc_2O_3 + 2SiO_2 \rightarrow Sc_2Si_2O_7 \quad (2)$$

$$Y_2O_3 + 2SiO_2 \rightarrow Y_2Si_2O_7 \quad (5)$$

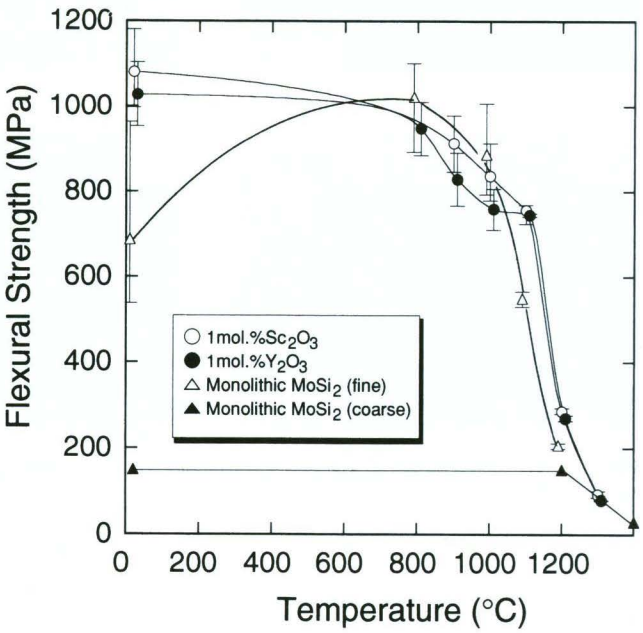

Fig. 8. Variation of flexural strength with temperature for $MoSi_2$–SiO_2–R_2O_3 system.

are $\Delta V = -18\%$ and -15%, respectively. Because almost no porosity is observed by SEM, the progress of the reactions (2) or (5), i.e., the removal of SiO_2, results in an increase in density. For higher additive content (10–20 mol%), the densities decrease, because the densities of unreacted Sc_2O_3 and Y_2O_3 are lower than that of $MoSi_2$.

The Young's modulus of polycrystalline $MoSi_2$ (440 GPa) is calculated from the single crystal.[35] On the other hand, that of glassy SiO_2 is much smaller (73 GPa).[41] To a first approximation, the monolithic $MoSi_2$ sintered body is composed of 8.5 vol% glassy SiO_2 phase and 91.5 vol% $MoSi_2$ phase, and the Young's modulus of the sintered body without pores is calculated as 386 GPa using the following equation:[50]

$$\ln E_{\text{sintered body}} = V_{SiO_2} \ln E_{SiO_2} + V_{MoSi_2} \ln E_{MoSi_2} \quad (6)$$

The value of 386 GPa, somewhat larger than the observed value of 372 GPa, is within a reasonable comparison. Then, on the second approximation, the effect of dispersion of the $Mo_{\leq 5}Si_3C_{\leq 1}$ phase is accounted for in the calculation. Recently, we investigated the properties of polycrystalline

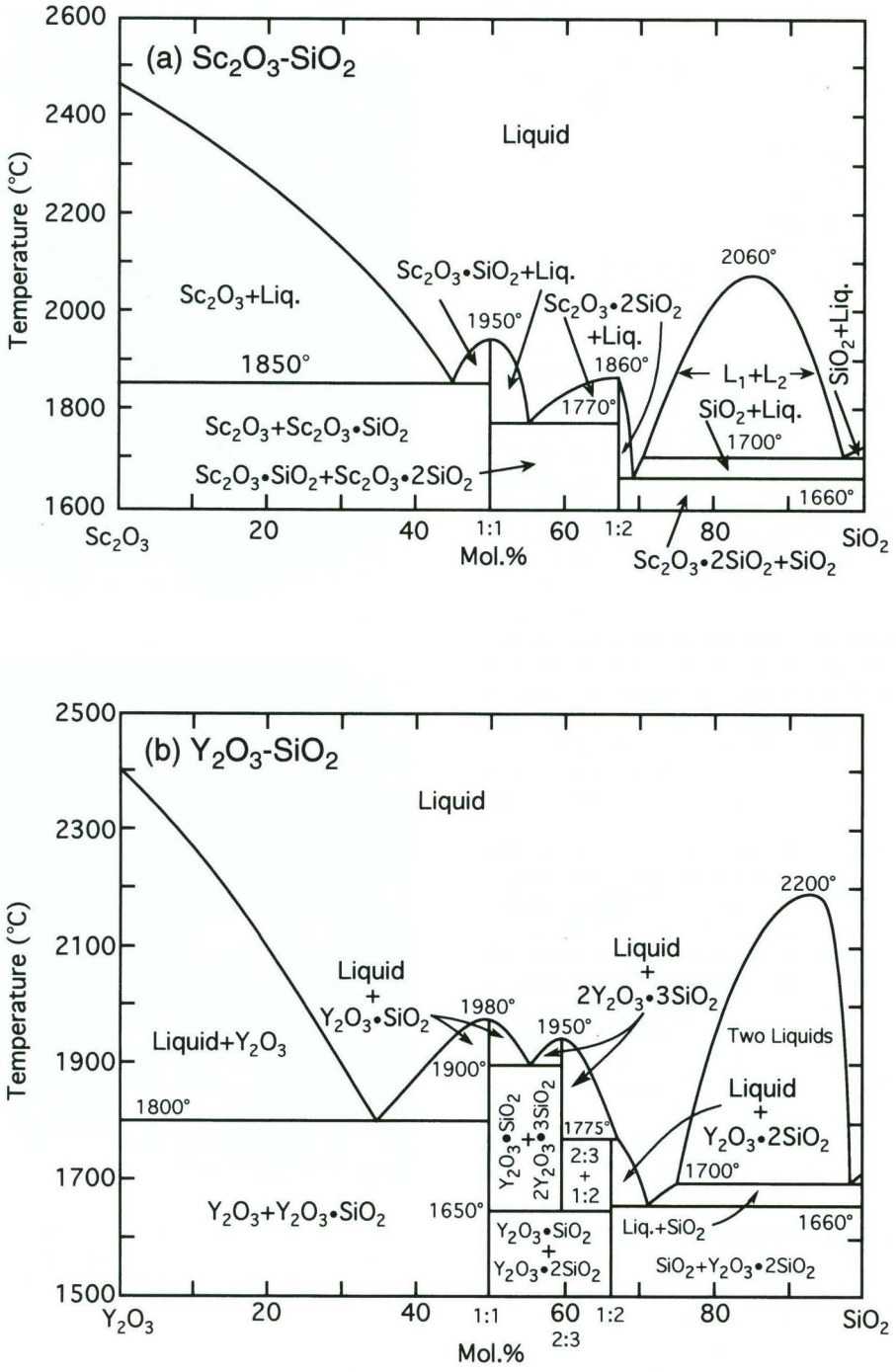

Fig. 9. Phase diagrams of (a) Sc_2O_3–SiO_2 and (b) Y_2O_3–SiO_2 binary systems.[21,22]

$Mo_{\leq 5}Si_3C_{\leq 1}$ phase and its composites.[47] The measured Young's modulus of polycrystalline $Mo_{\leq 5}Si_3C_{\leq 1}$ was 285 GPa. In this experiment, ~3 vol% of $Mo_{\leq 5}Si_3C_{\leq 1}$ phase is dispersed in the monolithic $MoSi_2$ sintered body. The Young's modulus of the $MoSi_2$ sintered body without pores is calculated using a modified equation:

$$\ln E_{\text{sintered body}} = V_{SiO_2} \ln E_{SiO_2} + V_{Mo\leq 5Si_3C\leq 1} \ln E_{Mo\leq Si_3C\leq 1} + V_{MoSi_2} \ln E_{MoSi_2} \quad (7)$$

where $V_{SiO_2} = 8.5\%$, $V_{Mo_{\leq 5}Si_3C_{\leq 1}} = 3.0\%$, and $V_{MoSi_2} = 88.5\%$. The calculated Young's modulus is 373 GPa and is in unusually close agreement with the observed value of 372 GPa.

The 5 mol% addition results in the maximum Young's modulus for both Sc_2O_3 and Y_2O_3 addition (Fig. 4). As is discussed above, free SiO_2 is minimized around this composition. Although there are no available reported values of the Young's modulus for $Sc_2Si_2O_7$, $Y_2Si_2O_7$, and other silicate phases, it is considered that the Young's modulus of such crystalline phases is surely higher than that of glassy SiO_2. $Sc_2Si_2O_7$ should have higher Young's modulus than $Y_2Si_2O_7$, because Sc^{3+} ion is smaller than Y^{3+} ion, with inevitably stronger Sc–O–Si bonds than Y–O–Si (as also confirmed by the effectively higher melting point). The Young's moduli of Sc_2O_3 and Y_2O_3 are 227.6 GPa[48] and 171.5 GPa,[49] respectively, suggesting again the stronger Sc–O versus Y–O bond (tracking mp at 2460°C versus 2400°C). Thus, the Young's modulus of Sc_2O_3-added system is always higher than that of Y_2O_3-added system. However, when the oxides are in excess at >5 mol%, Young's modulus of both $MoSi_2$–SiO_2–Sc_2O_3 and $MoSi_2$–SiO_2–Y_2O_3 systems inevitably drop.

Table V. Density and Young's Modulus of Phases Present[†]

Phase	Density (g/cm^3)[‡]	Young's modulus (GPa)[‡]
$MoSi_2$	6.270 [39]	440 [35]
$Mo_{\leq 5}Si_3C_{\leq 1}$	7.891 [40]	285 [47]
SiO_2 (glass)	2.20 [41]	73 [41]
Sc_2O_3	3.840 [42]	227.6 [48]
Y_2O_3	5.032 [43]	171.5 [49]
$Sc_2Si_2O_7$	3.394 [44]	
β-$Y_2Si_2O_7$	4.030 [45]	
Y_2SiO_5	4.441 [46]	

[†]$Y_4Si_3O_{12}$ data was not available. [‡]Numbers in brackets are Reference numbers.

(3) Microstructural Dependence of Mechanical Properties

As detailed in Section III, only a small amount of rare-earth oxide addition strongly improves various mechanical properties, e.g., 1 mol% additive significantly improves fracture strength. To illuminate the effect of crystallization on mechanical properties, a TEM observation on 1-mol%-Sc_2O_3-added system with the highest bending strength is shown in Figs. 10(a) and (b). Figure 10(a) shows a siliceous pocket in the sintered body, in which crystalline $Sc_2Si_2O_7$ has formed. Another siliceous pocket is indicated in Fig. 10(b); dislocation networks are observed in the $MoSi_2$ around the oxide pockets. The crystalline silicates appear to be less deformable than glassy SiO_2. Thus, thermal stress between matrix and oxides is not fully relaxed by the plastic deformation of glassy SiO_2, leading to numerous dislocations in the $MoSi_2$. When the pockets contain the crystalline silicates, more dislocations can be seen than in the case of noncrystalline or only slightly crystalline pockets.

For the 1–5 mol% addition, the amount of total oxide phase is not so large. Formed $R_2Si_2O_7$ crystals effectively toughen the glassy phase and improve mechanical properties, perhaps by reducing the source flaw size in the glass. With greater addition, however, the oxide phases become continuous and may act as larger fracture origins. Mechanical properties, especially strength, decline. In Fig. 5, the variation of five to six specimen tests becomes large at 10 mol% addition, equivalent to 14 and 17 vol% addition for Sc_2O_3 and Y_2O_3 addition, respectively (Table III). Thus, 10 mol% addition is at the threshold value of ~16 vol% for percolative contact of oxide phases and may well explain why the error bars increase at this level. These reasonings should be considered preliminary and tentative at this stage.

(4) Comparison with Other Techniques to Remove Glassy SiO_2

In the Introduction, SiO_2-removing techniques were classified into five categories. The present study on $MoSi_2$–SiO_2–Sc_2O_3 and $MoSi_2$–SiO_2–Y_2O_3 is in the same vein as our previous study on $MoSi_2$–SiO_2–ZrO_2.[8] This method is basically analogous to that used with Si_3N_4-based ceramics.[23–26] One difference, however, is that glassy SiO_2 and additive oxides in $MoSi_2$ do not form films at grain boundaries, concentrating at triple points, so that the reaction seems to progress easily under relatively mild conditions (1600°C for 1 h).

V. Conclusions

In this investigation, we examined the modification of the grain-boundary phase in $MoSi_2$ hot-pressed bodies by additions of Sc_2O_3 and Y_2O_3. In summary,

(1) The intergranular glassy SiO_2 phase was converted to the crystalline silicates.

(2) Mechanical properties at both room temperature and high temperatures were enhanced by Sc_2O_3 and Y_2O_3 addition, even at an amount as low as 1 mol%.

(3) These results indicate that *in-situ* crystallization of the glassy SiO_2 phase by the addition of refractory oxides holds promise for fabricating $MoSi_2$-based composites with improved mechanical properties, and further optimization can be expected.

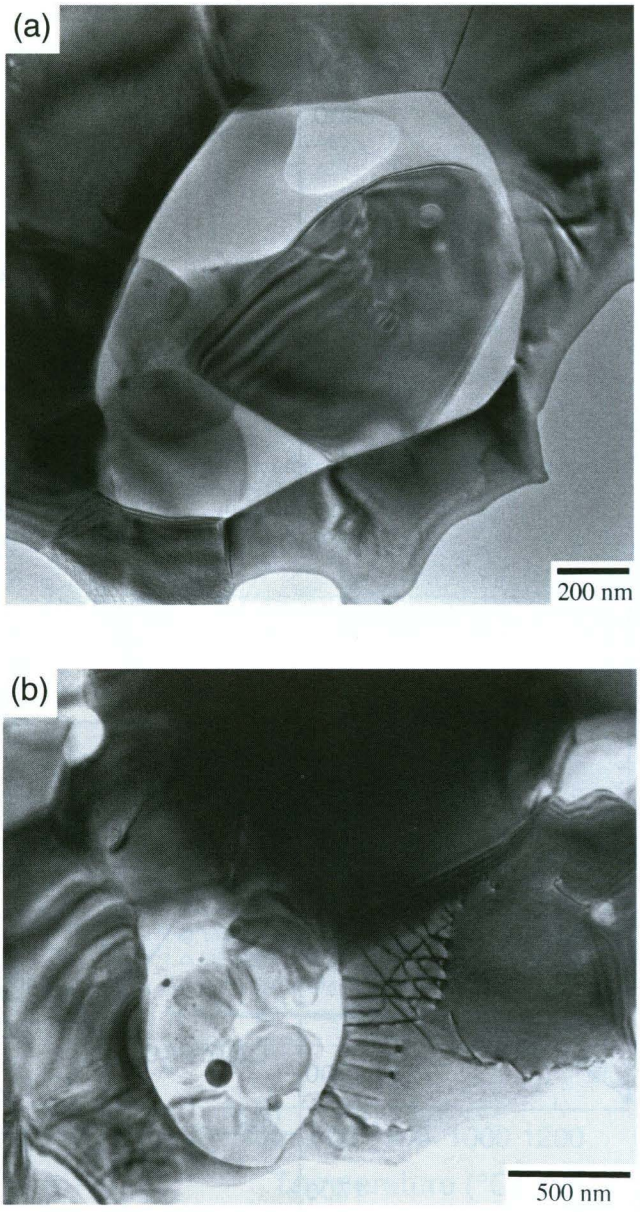

Fig. 10. TEM photographs of 1-mol%-Sc_2O_3-added $MoSi_2$: (a) $Sc_2Si_2O_7$ formation inside the glassy SiO_2 pocket (by EDS), and (b) dislocation networks around siliceous pockets.

Acknowledgment: The authors gratefully acknowledge Professor S. W. Lee at Sun Moon University for helpful discussions. We gratefully acknowledge Japan New Metals Co., Ltd. for kindly providing the $MoSi_2$ powder.

References

[1]A. K. Vasudévan and J. J. Petrovic, "A Comparative Overview of Molybdenum Disilicide Composites," *Mater. Sci. Eng.*, **A155**, 1–17 (1992).

[2]Y. L. Jeng and E. J. Lavernia, "Processing of Molybdenum Disilicide," *J. Mater. Sci.*, **29**, 2557–71 (1994).

[3]D. J. Evans, F. J. Scheltens, J. B. Woodhouse, and H. L. Fraser, "Deformation Mechanisms in $MoSi_2$ at Temperatures above the Brittle-to-Ductile Transition Temperature. I. Polycrystalline $MoSi_2$," *Philos. Mag. A*, **75** [1] 1–15 (1997).

[4]X. Fan, T. Ishigaki, and Y. Sato, "Phase Formation in Molybdenum Disilicide Powders during In-Flight Induction Plasma Treatment," *J. Mater. Res.*, **12** [5] 1315–26 (1997).

[5]A. Costa e Silva and M. J. Kaufman, "Phase Relations in the Mo-Si-C System Relevant to the Processing of $MoSi_2$–SiC Composites," *Metall. Mater. Trans.*, **25A**, 5–15 (1994).

[6]S. A. Maloy, A. H. Heuer, J. J. Lewandowski, and J. J. Petrovic, "Carbon Additions to Molybdenum Disilicide: Improved High-Temperature Mechanical Properties," *J. Am. Ceram. Soc.*, **74** [10] 2704–706 (1991).

[7]S. A. Maloy, J. J. Lewndowski, A. H. Heuer, and J. J. Petrovic, "Effects of Carbon Additions on the High Temperature Mechanical Properties of Molybdenum Disilicide," *Mater. Sci. Eng.*, **A155**, 159–63 (1992).

[8]Y. Suzuki, T. Sekino, and K. Niihara, "Effects of ZrO_2 Addition on Microstructure and Mechanical Properties of $MoSi_2$," *Ser. Metall. Mater.*, **33** [1] 69–74 (1995).

[9]Y. Suzuki, A. Nakahira, T. Sekino, and K. Niihara, "Microstructure and Mechanical Properties of Mo-Si-Al Alloy and Mo-Si-Al/SiC Composite," *J. Jpn. Soc. Powder and Powder Metall.*, **43** [3] 272–77 (1996).

[10]E. Fitzer and W. Remmele, "Oxidation of Molybdenum Disilicide"; pp. 19–42 in Ceramic Transactions, Vol. 10, *Corrosive and Erosive Degradation of Ceramics*. Edited by R. B. Tressler and M. McNallan. American Ceramic Society, Westerville, OH, 1989.

[11]R. Gibala, A. K. Ghosh, D. C. Van Aken, D. J. Srolovitz, A. Basu, H. Chang, D. P. Mason, and W. Yang, "Mechanical Behavior and Interface Design of $MoSi_2$-Based Alloys and Composites," *Mater. Sci. Eng.*, **A155**, 147–58 (1992).

[12]D. A. Hardwick, P. L. Martin, S. N. Patankar, and J. J. Lewandowski, "Processing–Microstructure–Property Relationships in Polycrystalline $MoSi_2$"; pp. 665–74 in *Structural Intermetallics*, Proceedings of the First International Symposium on Structural Intermetallics. Edited by R. Darolia, J. J. Lewandowski, C. T. Liu, P. L. Martin, D. B. Miracle, and M. V. Nathal. TMS, Warrendale, PA, 1993.

[13]K. Shobu, T. Watanabe, and K. Tsuji, "Effects of Mo_2B_5 Addition to $MoSi_2$ Ceramics" (in Jpn.), *J. Ceram. Soc. Jpn.*, **97** [10] 1311–14 (1989).

[14]J. Hojo, Y. Ishizaka, K. Kishi, and S. Umebayashi, "Microstructure and Properties $MoSi_2$ and $MoSi_2$–SiC Sintered Bodies Obtained from Fine Powders," *J. Jpn. Soc. Powder and Powder Metall.*, **42** [11] 1295–99 (1995).

[15]W. A. Maxwell, NACA Research Memorandum E52 B06, (1952).

[16]E. Fitzer, K. Reinmuth, and H. Schnabel, "Comparing and Sintering of Molybdenum Disilicide," *Arch. Eisenhüttenwesen*, **40** [11] 895–900 (1969).

[17]A. Costa e Silva and M. J. Kaufman, "Microstructural Modification of $MoSi_2$ through Aluminum Additions," *Scr. Metall. Mater.*, **29** [8] 1141–45 (1993).

[18]A. Costa e Silva and M. J. Kaufman, "Applications of *In-Situ* Reactions to $MoSi_2$-Based Materials," *Mater. Sci. Eng.*, **A195**, 75–88 (1995).

[19]A. Costa e Silva and M. J. Kaufman, "Synthesis of $MoSi_2$–Boride Composites through *In-Situ* Displacement Reactions," *Intermetallics*, **5**, 1–15 (1997).

[20]Y. Suzuki, T. Sekino, and K. Niihara, "Effects of Al Substitution and Nano-Sized SiC Dispersion on Microstructure and Mechanical Properties of $MoSi_2$" pp. 189–94 in *Frontier Nanostructured Ceramics*, Proceedings of the 6th Tohwa University International Symposium (Fukuoka, Japan, Oct. 1996). Edited by Y. Nagano. Tohwa University Press, 1996.

[21]E. M. Levin, C. R. Robbins, and H. F. McMurdie; Fig. 2384 in *Phase Diagrams for Ceramists*. Edited by M. K. Reser. American Ceramic Society, Columbus, OH, 1969.

[22]E. M. Levin, C. R. Robbins, and H. F. McMurdie; Fig. 2388 in *Phase Diagrams for Ceramists*. Edited by M. K. Reser. American Ceramic Society, Columbus, OH, 1969.

[23]P. E. D. Morgan, F. F. Lange, D. R. Clarke, and B. I. Davis, "A New Si_3N_4 Material: Phase Relations in the System Si-Sc-O-N and Preliminary Property Studies," *J. Am. Ceram. Soc.*, **64** [4] C77–C78 (1981).

[24]P. E. D. Morgan, "Si_3N_4 Ceramic Densified Using Sc_2O_3 and SiO_2," U.S. Pat. No. 4 401 768, 1983.

[25]M. L. Mecartney, "Enhanced Crystallization of a Glassy Phase in Silicon Nitride by the Addition of Scandia," *J. Am. Ceram. Soc.*, **70** [12] C-380–C-382 (1987).

[26]D.-S. Cheong and W. A. Sanders, "High-Temperature Deformation and Microstructural Analysis for Silicon Nitride–Scandium(III) Oxide," *J. Am. Ceram. Soc.*, **75** [12] 3331–36 (1992).

[27]E. N. Kulenko and B. I. Polyak, "Sintering of the Ceramics Belonging to the $MoSi_2$–Y_2O_3 and $MoSi_2$–SiC Systems," *Refractories*, **30**, 418–25 (1990).

[28]I. Ya. Zalkind, E. N. Kulenko, T. N. Morugova, A. I. Rekov, and G. A. Fomina, "Interaction of the Granular-Laminar Material $MoSi_2$–Y_2O_3 with Fuel Slag," *Teplofiz. Vys. Temp.*, **19** [6] 1285–92 (1981).

[29]S. Wada, "Increase of Oxygen Content in Si_3N_4 Powder During Ball Milling Using Alcohol as Solvent," *J. Ceram. Soc. Jpn.*, **104** [11] 1085–87 (1996).

[30]K. Niihara, R. Morena, and D. P. H. Hasselman, "Evaluation of K_{IC} of Brittle Solids by the Indentation Method with Low Crack-to-Indent Ratios," *J. Mater. Sci. Lett.*, **1** [1] 13–16 (1982).

[31]E. Parthé and W. Jeitschko, "A Neutron Diffraction Study of the Nowotny Phase $Mo_{\leq 5}Si_3C_{\leq 1}$," *Acta Crystallogr.*, **19**, 1031–37 (1965).

[32]W. E. Lee, C. H. Drummond III, G. E. Hilmas, and S. Kumar, "Microstructural Evolution in Near-Eutectic Yttrium Silicate Compositions Fabricated from a Bulk Melt and as an Intergranular Phase in Silicon Nitride," *J. Am. Ceram. Soc.*, **73** [12] 3575–79 (1990).

[33]T. R. Dinger, R. S. Rai, and G. Thomas, "Crystallization Behavior of a Glass in the Y_2O_3–SiO_2–AlN System," *J. Am. Ceram. Soc.*, **71** [4] 236–44 (1988).

[34]G. H. Meier and F. S. Pettit, "The Oxidation Behavior of Intermetallic Compounds," *Mater. Sci. Eng.*, **A153**, 548–60 (1992).

[35]M. Nakamura, S. Matsumoto, and T. Hirano, "Elastic Constants of $MoSi_2$ and WSi_2 Single Crystals," *J. Mater. Sci.*, **25**, 3309–13 (1990).

[36]W. D. Kingery, H. K. Bowen, and D. R. Uhlmann, *Introduction to Ceramics*, 2nd ed.; Ch. 15. Wiley, New York, 1976.

[37]Y. Suzuki and K. Niihara, "Effect of SiC Reinforcement on Microstructure and Mechanical Properties of $MoSi_2$," *Sci. Eng. Comp. Mater.*, **6** [2] 85–94 (1997).

[38]D. H. Carter, W. S. Gibbs, and J. J. Petrovic, "Mechanical Characterization of SiC Whisker-Reinforced $MoSi_2$"; pp. 977–86 in *Proceedings of Ceramic Materials and Components for Engines*. Edited by V. J. Tennery. American Ceramic Society, Westerville, OH, 1998.

[39]Powder Diffraction File, Card. No. 41-0612. International Centre on Diffraction Data, Newtowne Square, PA, 1991.

[40]Powder Diffraction File, Card. No. 43-1199. International Centre on Diffraction Data, Newtowne Square, PA, 1993.

[41]H. Yanagida *et al.* (Eds.) *Cyclopedia of Fine Ceramics*; pp. 135–53. Gihodo Press, Tokyo, Japan, 1987.

[42]Powder Diffraction File, Card. No. 43-1028. International Centre on Diffraction Data, Newtowne Square, PA, 1993.

[43]Powder Diffraction File, Card. No. 43-1036. International Centre on Diffraction Data, Newtowne Square, PA, 1993.

[44]Powder Diffraction File, Card. No. 20-1037. International Centre on Diffraction Data, Newtowne Square, PA, 1970.

[45]Powder Diffraction File, Card. No. 38-0440. International Centre on Diffraction Data, Newtowne Square, PA, 1988.

[46]Powder Diffraction File, Card. No. 36-1476. International Centre on Diffraction Data, Newtowne Square, PA, 1986.

[47]Y. Suzuki and K. Niihara, "Synthesis and Mechanical Properties of $Mo_{\leq 5}Si_3C_{\leq 1}$ and $Mo_{\leq 5}Si_3C_{\leq 1}$-Based Composites," *Intermetallics*, **6** [1] 7–13 (1998).

[48]S. L. Dole, O. Hunter Jr., and F. W. Calderwood, "Elastic Properties of Polycrystalline Scandium and Thulium Sesquioxides," *J. Am. Ceram. Soc.*, **60** [3–4] 167–68 (1977).

[49]W. R. Manning, O. Hunter Jr., and B. R. Powell Jr., "Elastic Properties of Polycrystalline Yttrium Oxide, Dysprosium Oxide, Holmium Oxide, and Erbium Oxide: Room-Temperature Measurements," *J. Am. Ceram. Soc.*, **52** [8] 436–42 (1969).

[50]Y. Kagawa and H. Hatta, *Tailoring Ceramic Composites*; pp. 96–119. Agune Shoufusya, Tokyo, Japan, 1990. □